

Article

Water Based Synthesis of ZIF-8 Assisted by Hydrogen Bond Acceptors and Enhancement of CO₂ Uptake by Solvent Assisted Ligand Exchange

Kasama Kenyotha, Kingkaew Chayakul Chanapattarapol * , Sirirath McCloskey and Phongphan Jantaharn

Materials Chemistry Research Center, Department of Chemistry and Center of Excellence for Innovation in Chemistry, Faculty of Science, Khon Kaen University, Khon Kaen 40002, Thailand;

kasama_ken@kkumail.com (K.K.); sirsod@kku.ac.th (S.M.); Phongphanjantaharn@gmail.com (P.J.)

* Correspondence: kingkaew@kku.ac.th; Tel.: +66-430-09700 (ext. 12371); Fax: +66-432-02373

Received: 28 April 2020; Accepted: 4 July 2020; Published: 10 July 2020



Abstract: The aim of this work was to synthesize zeolitic imidazolate framework-8 (ZIF-8) by an alternative method and then modify the surface properties for enhancing the CO₂ adsorption performance. The ZIF-8 was synthesized by a water based synthesis method using 2-methyl imidazole (2-MeIM) as a hydrogen bond donor and quaternary ammonium salts (QAS) as a hydrogen bond acceptor. The optimal synthesis conditions were investigated by varying (i) the order of precursor mixing during the synthesis process (ii) different QAS (tetrabutyl ammonium bromide (TBAB), tetraethyl ammonium bromide (TEAB) and trimethyl phenyl ammonium bromide (TMPAB)) and (iii) the ratio between 2-MeIM and QAS. The results show that the optimal synthesis condition was using TMPAB as the hydrogen bond acceptor with the ratio between 2-MeIM and TMPAB of 8:2 and in the order of first mixing both hydrogen bond donor and acceptor before adding Zn(NO₃)₂·6H₂O solution. TMPAB can provide uniform size distribution with the smallest particle sizes of ZIF-8. This can be explained by the higher hydrogen bond strength between hydrogen bond donor (2-MeIM) and hydrogen bond acceptor (TMPAB) when compared with that of the rest of two QAS. The synthesized ZIF-8 was modified by solvent-assisted ligand exchange methods. The organic linker of ZIF-8 (2-MeIM) was exchanged by 2-aminobenzimidazole (2-NH₂bZIM) and 2-phenylimidazole (2-PhIM). The CO₂ uptake of modified ZIF-8 was enhanced upon exchanging with 2-NH₂bZIM. The increase in CO₂ uptake was due to an additional interaction between CO₂ and exchanged imidazole linker and an increase in surface properties (higher surface area, pore size and pore volume).

Keywords: CO₂ uptake; ZIF-8; water based synthesis; solvent-assisted ligand exchange

1. Introduction

In recent years, global warming and climate change have become the most important problems facing humanity. These phenomena are caused by large amounts of greenhouse gases emission into the atmosphere. Carbon dioxide (CO₂) is one of the greenhouse gases which is mainly generated from burning fossil fuels in industrial processes for the generation of energy and transportation. Therefore, a decrease in CO₂ emissions is needed, which can be achieved by reducing fossil fuel burning and by capturing CO₂ from the atmosphere. Various technologies are used for capturing CO₂, such as cryogenic separation [1–3], CO₂ membrane-based separation [4–6], chemical absorption [7–9] and adsorption technology [10–12]. Solid adsorption technology is now of interest due to its many advantages, such as energy-efficiency, low prices and the ease by which it can be modified. Several solid adsorbents which are porous have been studied for CO₂ adsorption, such as zeolites [13–15] metal

organic frameworks (MOFs) [16–18] and zeolitic imidazole frameworks (ZIFs) [19–21]. Among these adsorbents, ZIFs are candidate adsorbents for gas adsorption because they exhibit many advantageous properties, such as high stability, high specific surface area, and high porosity. It also exhibits functional adjustability, which can lead to increasing CO₂ adsorption capacity. ZIFs are generated by transition metal atoms coordinated with four molecules of imidazole linker forming a tetrahedral molecular structure. These tetrahedral shapes can be formed into three-dimensional frameworks and porous crystalline materials are obtained. Among the ZIFs materials, ZIF-8 is of interest due to its low toxicity, and it is a very robust material when compared with other transition metals.

ZIF-8 can be prepared by many different methods which can affect its surface properties. Mostly, solvothermal [22–24] and hydrothermal (or water based synthesis) [25–27] methods were used because of their simplicity and usually provide high surface area. For solvothermal method, general organic solvents used are *N,N*-dimethylformamide (DMF), *N*-methylpyrrolidine, and *N,N*-diethylformamide. However, those organic solvents were difficult to remove from the pores of ZIF-8, and thus, methanol is a more popular solvent for ZIF-8 synthesis by this method [28]. The solvothermal method can provide ZIF-8 with desired properties, but using an excessive organic solvent becomes disadvantageous since the organic solvent is flammable, expensive, toxic and environmentally harmful. Therefore, to overcome this problem, the green synthesis method is needed. In recent years, the synthesis of ZIF-8 by using an aqueous solution has been of interest and has become an alternative approach which is called water based synthesis method. In the case of the synthesis process which was performed in water above the normal boiling point and under autogenous pressure, this can be specifically called as hydrothermal method. In the water based synthesis route, 2-methylimidazole (2-MeIM) can be deprotonated by an aqueous solvent (water), and the deprotonated 2-MeIM is further coordinated with Zn²⁺ to form a ZIF-8 framework. It has been reported that the deprotonation rate of 2-MeIM affected the nucleation rate and growth of ZIF-8, which allowed the ZIF-8 crystallinity and morphology to be controlled [29–31]. The deprotonation of 2-MeIM can be facilitated by the formation of hydrogen bonding between 2-MeIM (hydrogen bond donor) and quaternary ammonium salts; QAS (hydrogen bond acceptor). A high deprotonation rate of 2-MeIM would lead to a high nucleation rate of ZIF-8, which also leads to the controlling of crystalline growth. In order to increase the hydrogen bond strength between these two compounds, an appropriate hydrogen bond acceptor must be used. Quaternary ammonium salts were reported as a hydrogen bond acceptor (or deprotonated agent) to be used which can be formed hydrogen bonding to 2-MeIM. In addition, in order to enhance CO₂ adsorption capacity, it is necessary to add an active site on the ZIF-8 surface. A solvent-assisted ligand exchange (SALE) method is an alternative method for material synthesis as it is used to replace or exchange the functional group on the MOFs linker which can lead to an increase in some properties, such as improving the catalytically active site [32,33], increasing proton conduction [34], increasing photochemical H₂ production [35], controlling over-catenation [36] and increasing CO₂ adsorption [37]. In this method, the organic linker in the framework was replaced by its derivative for modifying their properties. In the ZIF-8 case, 2-methylimidazole linkers in the structure can be replaced by the derivative of imidazole in which their functional group can interact more with CO₂ than the old single linker.

In this work, ZIF-8 was synthesized by the water based synthesis method assisted by hydrogen bond acceptors (QAS) to facilitate deprotonation of hydrogen bond donor (2-MeIM) for controlling the ZIF-8 properties (size, surface properties and morphology). The effect of synthesis conditions on ZIF-8 properties were studied, which included the effects of order of precursor mixing, different hydrogen bond acceptors (QAS) and the ratio between 2-MeIM and QAS. Moreover, synthesized ZIF-8 by an optimal synthesis condition was modified by solvent-assisted ligand exchanging in order to increase CO₂ adsorption capacity. Synthesized ZIF-8 was characterized by several techniques, such as X-ray diffraction (XRD), scanning electron microscopy (SEM), N₂ adsorption-desorption, nuclear magnetic resonance (NMR) and CO₂ uptake measurement by thermogravimetric analysis (TGA).

2. Materials and Methods

2.1. Materials

All chemicals in this experiment were of analytical grade without further purification. Zinc(II)nitrate hexahydrate ($Zn(NO_3)_2 \cdot 6H_2O$; 98%) was purchased from Sigma-Aldrich, while 2-methyl imidazole (2-MeIM; 99+%) was purchased from Acros Organics. Three quaternary ammonium salts (QAS), tetrabutyl ammonium bromide (TBAB; 99+%), tetraethyl ammonium bromide (TEAB; 99%) and trimethyl phenyl ammonium bromide (TMPAB; 98%), were purchased from Across Organics, Merck, and Sigma-Aldrich, respectively. Two imidazole derivatives: 2-aminobenzimidazole (2-NH₂bZIM; 99+%) and 2-phenylimidazole (2-PhIM; 99+%) were purchased from Acros Organics. Methanol and n-butanol were purchased from Carlo and RCL Labscan, respectively. Deionized water was used for all synthesized processes.

2.2. ZIF-8 Synthesis by Water Based Synthesis Assisted by Hydrogen Bond Acceptors

The molar ratio of precursor between $Zn(NO_3)_2 \cdot 6H_2O$ and 2-MeIM was kept constant at 1:4. The effect of synthesis conditions on ZIF-8 properties were investigated. First, the effects of changing the ordering steps of precursor mixing were studied by using two different routes. For route no.1, $Zn(NO_3)_2 \cdot 6H_2O$ (0.86 g, 0.00289 mol), 2-MeIM (0.95 g, 0.0116 mol) and TMPAB (0.62 g, 0.0287 mol) (TMPAB was selected as representative QAS sources) were mixed and heated under stirring for 30 min or until the precursor turned into a homogeneous solution. Then, the deionized water (50 mL, 2.8 mol) was added and the mixture was continuously stirred for 30 min; in this step, the solution turned turbid. After that, the mixture was centrifuged at 6000 rpm for 10 min, after which the white precipitates were obtained. The precipitant was washed with deionized water several times. Finally, the solid sample was dried at 120 °C for 24 hours. For route no.2, 2-MeIM and QAS were first mixed and heated under continuous stirring for 30 min or until a homogeneous solution was obtained. $Zn(NO_3)_2 \cdot 6H_2O$ which was dissolved in 50 mL of deionized water was added into the former solution and stirred for 30 min. After that, the synthesis procedure was carried out by the same process as route no.1. Second, the effects of different types of QAS were studied by using three different sources (tetrabutyl ammonium bromide (TBAB), tetraethyl ammonium bromide (TEAB) and trimethyl phenyl ammonium bromide (TMPAB)). The ratio between 2-MeIM and QAS was kept constant at 8:2. In synthesis procedure, 2-MeIM and QAS were first mixed together to form a homogeneous solution before the addition of the zinc nitrate solution. The temperature at homogeneous point was defined as synthesis temperature. The synthesis temperature of 2-MeIM and TBAB, TEAB and TMPAB were 109.0, 80.0 and 120.0 °C, respectively. Third, the effects of various ratios between 2-MeIM and QAS were studied by varying the ratios of these two precursors, at 4:6, 5:5, 6:4, 7:3 and 8:2.

Moreover, ZIF-8 was also synthesized by the solvothermal method for comparison with synthesized ZIF-8 by the above method. The molar ratio between Zn precursor and 2-MeIM was 1:4, and methanol was used as a solvent. First, $Zn(NO_3)_2 \cdot 6H_2O$ and 2-MeIM were separately dissolved in methanol and stirred until the precursors were completely dissolved. Second, two solutions were mixed and continuously stirred for 1 hour. The mixture was centrifuged at 6000 rpm for 20 min to obtain the white precipitates. The solid was filtered and washed with deionized water and methanol, respectively. Finally, the solid sample was dried at 80 °C for 24 hours.

2.3. Modification of Synthesized ZIF-8 by Solvent-assisted Ligand Exchange (SALE) Method

In this modification method, 2-MeIM linker in synthesized ZIF-8 was exchanged with two imidazole derivatives (2-NH₂bZIM and 2-PhIM). The preparation details followed C. W. Tsai et al. [37]. Briefly, 100 mg of synthesized ZIF-8 was dispersed in methanol for 3 min under ultrasonic probe. Then the solution was transferred into a polypropylene bottle. At the same time, the imidazole derivatives were also dissolved in appropriate solvents (methanol and n-butanol for 2-NH₂bZIM and 2-PhIM, respectively). The imidazole derivative solution was then added into the ZIF-8 solution and the

mixture was heated at 60 °C for 3 days to exchange the linker. After cooling the solution, the obtained solid was washed by methanol and then separated by centrifugation at 6000 rpm for 15 min. Finally, the modified ZIF-8 was obtained by drying at 60 °C for 24 hours. The effect of molar ratio between synthesized ZIF-8 and imidazole derivatives were varied at 1:1, 1:3 and 1:5.

2.4. Characterization

To confirm and identify the structures of synthesized and modified samples, powder X-ray diffraction (PXRD) patterns were obtained by a PANalytical Empyrean X-ray diffractometer (Malvern Panalytical, Malvern, UK). The 2θ was operated in the range of 5° to 50°.

The morphology of synthesized and modified ZIF-8 was determined by a LEO 1450VP scanning electron microscope (SEM) (Carl Zeiss AG, Oberkochen, Germany). The powder sample was prepared before scanning by dispersing it on carbon tape that was put on a specimen stub. After that, the sample was coated with a thin layer of gold by low-vacuum sputter coating to reduce the electron charge.

The surface and porosity properties (surface area, pore volume and average pore size) of synthesized and modified samples were determined by measuring the nitrogen adsorption/desorption isotherm at 77 K by Bel Sorp mini II (MicrotracBEL Corp., Osaka, Japan) The sample was degassed at 120 °C for 5 hours before the adsorption/desorption process to remove water molecules or impure molecules from the sample surface. The BET equation was used to calculate the specific surface area at a relative pressure (P/P_0) range between 0 and 0.1. The pore volume of samples was determined at the relative pressure close to unity ($P/P_0 \approx 1$).

Fourier transform infrared (FTIR) spectra of synthesized ZIF-8 sample were obtained by the Bruker (TENSOR27) spectrometer (Bruker Corp., Billerica, MA, USA) using the KBr pellet method. The measurement range was 4000–400 cm^{-1} .

To evidence the exchange achieved during the SALE process, the modified samples were analyzed by digestive liquid $^1\text{H-NMR}$ in which acetic acid-*d*4 was used as a solvent. $^1\text{H-NMR}$ spectra were obtained by Bruker AVANCE III 500 MHz (Bruker Corp., Billerica, MA, USA).

2.5. CO_2 Adsorption Study

The adsorption measurement was performed using Pyris Diamond TG/DTA Perkin Elmer Analysis. The CO_2 uptake was measured at 40 °C and ambient pressure. The surface of synthesized ZIF-8 was pre-treated by heating (heating rate 10 °C/min) the sample at 150 °C under purging of N_2 for 45 min (flow rate 100 mL/min). After the pretreatment process, the sample was cooled down to 40 °C under N_2 atmosphere. After that, pure CO_2 was then switched to the sample to start the gas uptake process and the CO_2 uptake was proceeded for 95 min. Upon decreasing the temperature, the weight of the sample increased due to the adsorption of CO_2 on the solid surface. The CO_2 uptake can be calculated by differentiating the weight before and after adsorption.

3. Results and Discussion

3.1. ZIF-8 Synthesis by Water Based Synthesis Assisted by Hydrogen Bond Acceptors

3.1.1. Effect of Mixed Ordering Step on ZIF-8 Properties

All precursors were mixed together under heating and stirring to form a final product. However, the order of precursor mixing also dominated the obtained samples. Therefore, the effect of the order of mixing between the precursors on ZIF-8 properties was investigated by using two different routes; route 1 and 2. For route 1, all precursors ($\text{Zn}(\text{NO}_3)_2 \cdot 6\text{H}_2\text{O}$, 2-MeIm and TMPAB) were mixed together under heating and stirring. After that, deionized water was subsequently added to precipitate the product. For route 2, 2-MeIm and QAS were firstly mixed and the $\text{Zn}(\text{NO}_3)_2 \cdot 6\text{H}_2\text{O}$ solution was then added. Figure 1 illustrates the XRD patterns of synthesized ZIF-8 obtained from routes 1 and 2 compared with that from solvothermal method. It is clearly seen that only the synthesized sample

by route 2 can provide the characteristic peaks of ZIF-8 which is in accordance with ZIF-8 by the solvothermal method. However, ZIF-8 cannot be formed by route 1. Consequently, the optimum method for the mixing sequence of precursors was route 2. Moreover, the role of QAS was also investigated by synthesizing ZIF-8 without the addition of QAS. The results show that ZIF-8 cannot be produced without adding QAS by this synthesis procedure, as illustrated in XRD patterns in Figure 1 (2-MeIM: Zn²⁺ sample). This indicated that QAS acts as a template for ZIF-8 formation during the synthesis process [31].

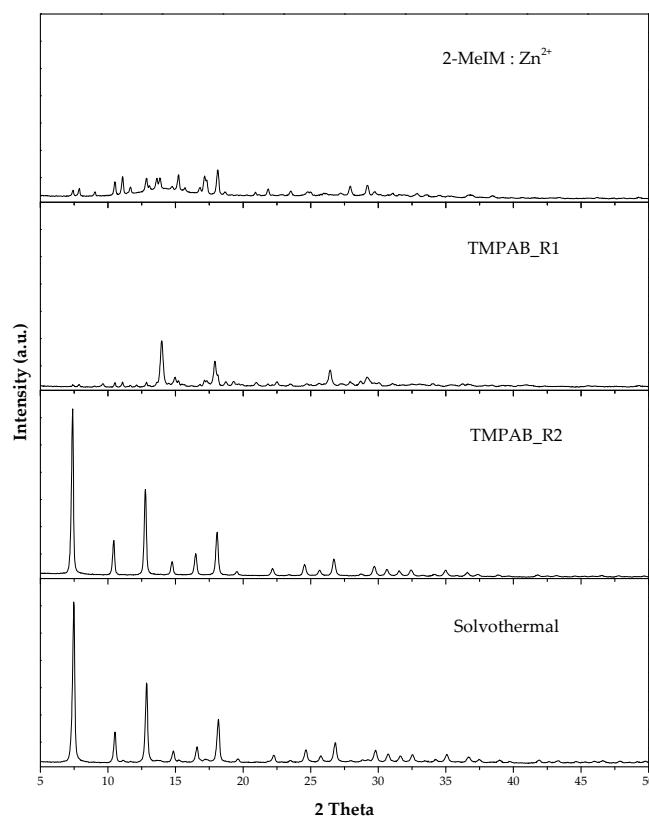


Figure 1. XRD patterns of synthesized zeolitic imidazolate framework-8 (ZIF-8) samples obtained from route 1 (R1) and route 2 (R2) compared with solvothermal method.

3.1.2. Effect of Different Quaternary Ammonium Salts

From the previous part, the optimal mixing order of precursors was route 2, i.e., the organic linker and QAS were first mixed and Zn(NO₃)₂·6H₂O solution was then added. In this part, the effects of different quaternary ammonium salts on ZIF-8 properties were investigated. Figure 2 displays XRD patterns of synthesized samples obtained from three different QAS: tetrabutyl ammonium bromide, tetraethyl ammonium bromide and trimethyl phenyl ammonium bromide. At the same ratio between 2-MeIM and QAS (8:2), tetraethyl ammonium bromide, tetrabutyl ammonium bromide and trimethyl phenyl ammonium bromide yielded ZIF-8 with different crystallinities. Synthesized ZIF-8 obtained from TMPAB gave the highest characteristic peak intensities of ZIF-8, which can attribute to high crystallinity. The SEM results confirmed the phase, crystal shape and morphologies of all synthesized samples. Figure 3 displays SEM images of ZIF-8 obtained from three different QAS. ZIF-8 obtained from tetraethyl ammonium bromide and tetrabutyl ammonium bromide exhibited an irregular shape with a high degree of agglomeration. While ZIF-8 obtained from trimethyl phenyl ammonium bromide showed a well distributed particle of truncated rhombic dodecahedra shape with a significant reduction in particle size lower than that of ZIF-8 obtained from both former QAS. Therefore, TMPAB was selected to be used as the QAS (hydrogen bond acceptor) for the further synthesis process in the next part.

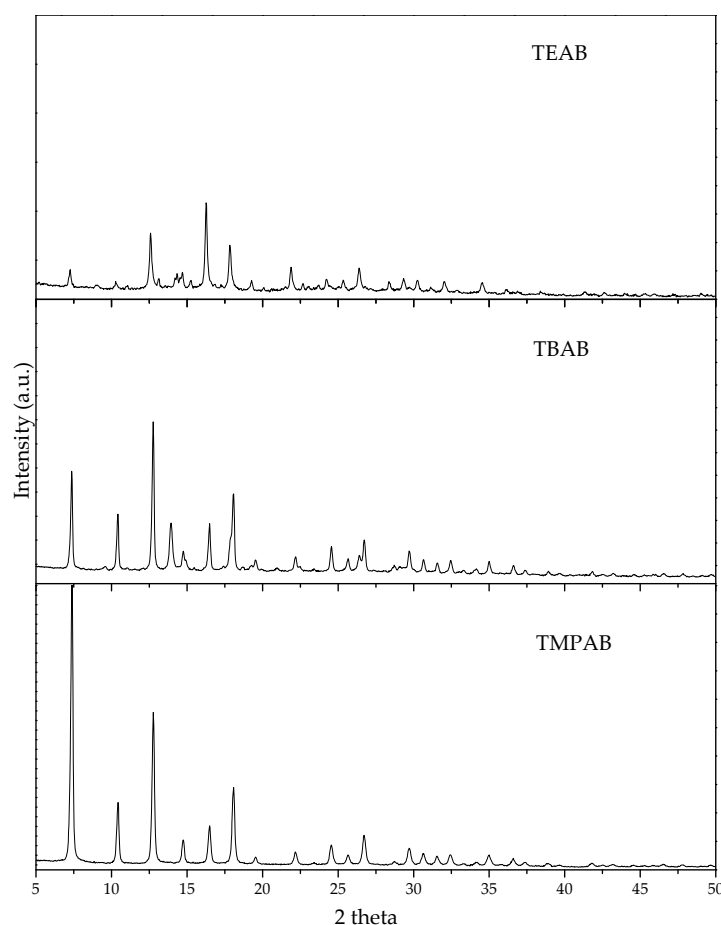


Figure 2. XRD patterns of synthesized samples obtained from different quaternary ammonium salts. The ratio between 2-methyl imidazole (2-MeIM) and quaternary ammonium salts (QAS) was 8:2.

The role of quaternary ammonium salts in synthesis process was to accelerate the deprotonation of 2-MeIM and the deprotonated 2-MeIM was further coordinated with the metal ion (Zn^{2+}) and forming the framework [31]. This effect can accelerate the nucleation and crystal growth rate. Finally, ZIF-8 with a uniform distribution of particle sizes was produced. The deprotonation can be accelerated by facilitating withdrawing the hydrogen atom from 2-MeIM, which can be done by forming a hydrogen bond with a hydrogen bond acceptor. In this work, 2-methyl imidazole acted as a hydrogen bond donor, while quaternary ammonium salts played a role as a hydrogen bond acceptor. Three quaternary ammonium salts had different hydrogen bond acceptor properties due to their different structures. Therefore, hydrogen bonding between 2-MeIM and QAS was also different. The hydrogen bond strength between these two precursors can dominate the deprotonation of the hydrogen bond donor (2-MeIM) and thus the nucleation and crystal growth of ZIF-8 can be controlled.

Hydrogen bonding is an attractive interaction between hydrogen bond donor (denoted as HX) and hydrogen bond acceptor (denoted as Y); thus, hydrogen bonding can be expressed as $XH \cdots Y$, where X is an electronegative atom, such as O, N or F, and Y can be any electron rich atom. C. Laurence and M. Berthelot [38] studied the strength of hydrogen bond acceptors (HBAs) by measuring from the Gibbs energy change for the formation of 1:1 hydrogen bonding complexes between hydrogen bond acceptors (bases) and a reference hydrogen bond donor (4-fluorophenol) in CCl_4 at 298 K. They concluded that the HBA strength depended on three factors: (i) the acceptor atom position in the periodic table; (ii) the polarizability and resonance effect of substituents around the acceptor atom; and (iii) the steric hindrance of the acceptor site.

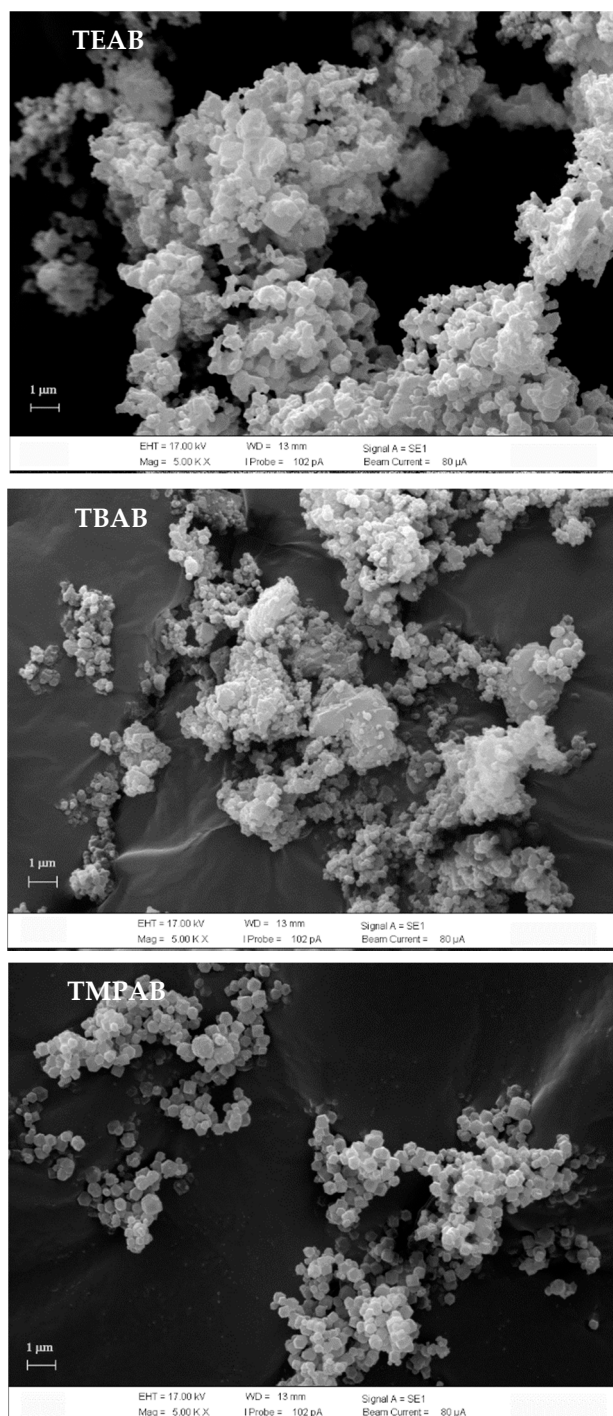


Figure 3. SEM images of ZIF-8 obtained from different quaternary ammonium salts.

Figure 4 illustrates the structure of three quaternary ammonium salts. The hydrogen bonding between 2-MeIM and these three QAS occurred at the bromine ion (Br^-) site. Therefore, Br^- ion is an acceptor site. Since three ammonium bromide salts had a different substituents group around Br^- ion, their hydrogen bond strength to 2-MeIM must be also different. Because the hydrogen bond donor was 2-MeIM and the hydrogen bond acceptors were varied (TEAB, TBAB and TMPAB), the hydrogen bond strength depended on the hydrogen bond acceptor strength (HBAs).

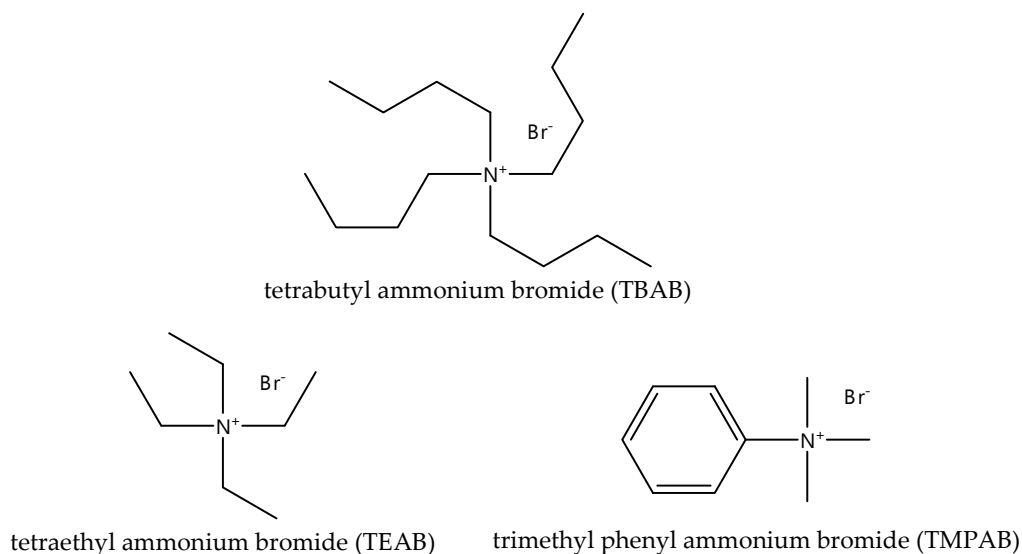


Figure 4. Structure of three quaternary ammonium salts.

The results from Figures 2 and 3 show that ZIF-8 obtained by using TMPAB exhibited the most uniform size distribution with the smallest particle size when compared with the other two QAS. This can be explained by the different substituent groups around the acceptor atom which dominated the hydrogen bond strength. Since the hydrogen bonding of 2-MeIM with three QAS occurred at the same acceptor site (Br⁻ ion), the substituent groups around bromine ions must dominate the hydrogen bond strength. The substituents functional groups around bromine ions was the ammonium group. This ammonium group also had different substituents functional groups, i.e., alkane for both TEAB and TBAB and methyl with phenyl groups for TMPAB. Considering the steric effect, TMPAB had the lowest steric hindrance around the Br⁻ ion when compared with TEAB and TBAB. Therefore, TMPAB should exhibit the highest hydrogen bond strength with 2-MeIM. Besides this interaction at the Br⁻ ion acceptor site, an additional interaction between TMPAB and 2-MeIM was also reported, i.e., interaction between phenyl group and 2-MeIM. M. Levitt and M. F. Perutz [39] reported that aromatic rings can act as hydrogen bond acceptors. They revealed that there is a significant interaction between a hydrogen bond donor (such as NH group) and the center (π -electron) of a benzene ring, which acts as a hydrogen bond acceptor. Therefore, the phenyl group in TMPAB can also interact with 2-MeIM by hydrogen bonding as mentioned above. Consequently, hydrogen bonding between 2-MeIM and TMPAB can occur at both Br⁻ ion and phenyl acceptor sites, as shown in Figure 5. From these reasons, using TMPAB to promote the deprotonation of 2-MeIM can provide the ZIF-8 with high uniform size distribution and the smallest ZIF-8 particle sizes. Figure 5 illustrates the proposed ZIF-8 formation mechanism with the use of trimethyl phenyl ammonium bromide (TMPAB) as a hydrogen bond acceptor. The hydrogen bonding between 2-MeIM can occur at two acceptor sites; the Br⁻ ion and π -electron sites. From this effect, the hydrogen bond strength was increased and the deprotonation of 2-MeIM was promoted. Therefore, the formation of ZIF-8 framework by coordination of deprotonated 2-MeIM and Zn²⁺ ion was also accelerated and finally the well size distribution of ZIF-8 particle was controlled and obtained. These results indicate that the additional hydrogen bonding between the π -electron site of benzene ring in TMPAB and 2-MeIM played an important role in enhancing the hydrogen bond strength and resulted in increasing the deprotonation of 2-MeIM process. On the other hand, from the results of XRD and SEM, ZIF-8 obtained from TBAB exhibited higher crystallinity than that of TEAB. This due to the TBAB structure which is more sterically hindered than TEAB and can lead to less association between the negative Br⁻ ion and the positive N atom in its structure; therefore, the Br⁻ ion was more available for bonding with 2-MeIM.

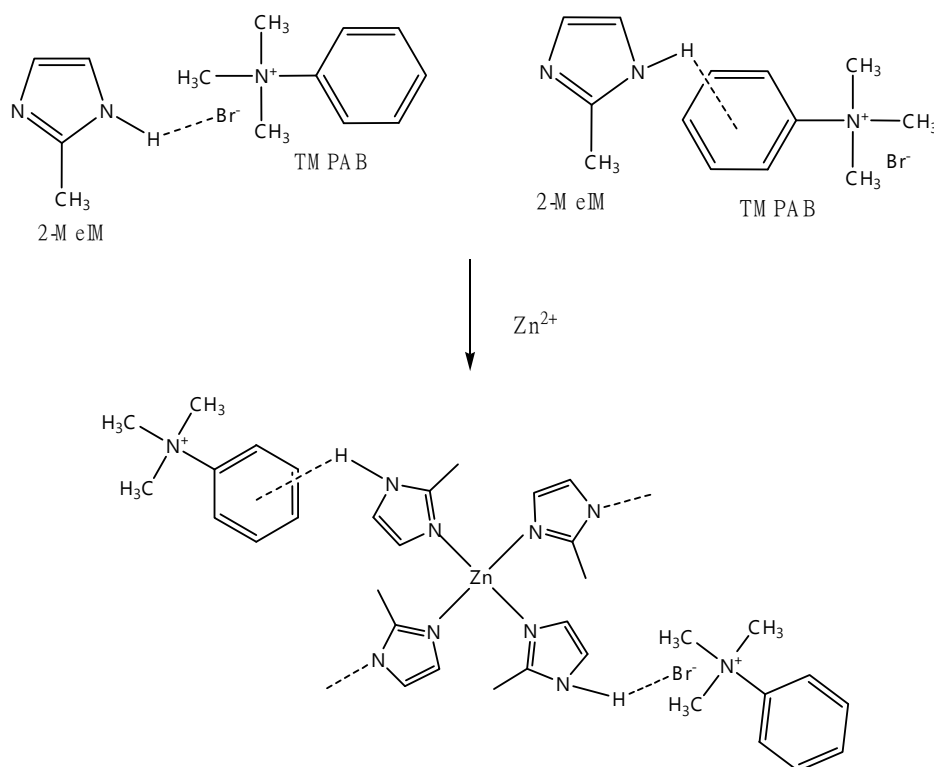


Figure 5. Proposed ZIF-8 formation mechanism with the use of trimethylphenyl ammonium bromide (TMPAB) as hydrogen bond acceptor.

3.1.3. Effect of Ratio between 2-MeIM and QAS

In this part, the ratio between 2-MeIM and TMPAB was varied at 5:5, 6:4, 7:3 and 8:2. It is noteworthy that the ratio between these two precursors at 4:6 cannot provide the desired product. From Figure 6, it is seen that all ratios exhibited ZIF-8 characteristic peaks with different intensities. Figure 7 shows SEM images of synthesized ZIF-8 for all ratios. The particle size of synthesized ZIF-8 was reduced upon lowering the QAS content. The particle size distribution of all samples is also displayed in the inset of each image. The size distributions were in the range of 500–1500 nm for 5:5, 6:4 and 7:3, while uniform size distribution of particle sizes of 400–600 nm was found for the sample with the ratio of 8:2.

In order to confirm the bonding in synthesized ZIF-8, ZIF-8 obtained from an optimal synthesis condition was used as a representative for all ZIF-8 samples. Figure 8 illustrates FTIR of original ZIF-8 synthesized by water based synthesis assisted by hydrogen bond acceptors (the ratio between 2-MeIM and TMPAB as 8:2). It was found that the infrared (IR) spectra of the ZIF-8 sample was in a good agreement with other works [40,41]. The peak at 423 cm^{-1} was assigned as Zn-N stretching vibration. The 690 cm^{-1} peak was attributed to the ring out of plane bending vibration of 2-MeIM. The 998 and 762 cm^{-1} peaks were due to C-N bending vibration and C-H bending mode. The peak at 1140 cm^{-1} was due to an aromatic C-N stretching mode, while the peak at 1607 cm^{-1} resulted from C=N stretching vibration. The peaks around 1305 to 1436 cm^{-1} were assigned as entire ring stretching, and the peak at 1513 cm^{-1} was due to the C=C stretching mode. The peaks at 2917 and 3100 cm^{-1} were attributed as aliphatic and aromatic C-H stretching of methyl imidazole, respectively.

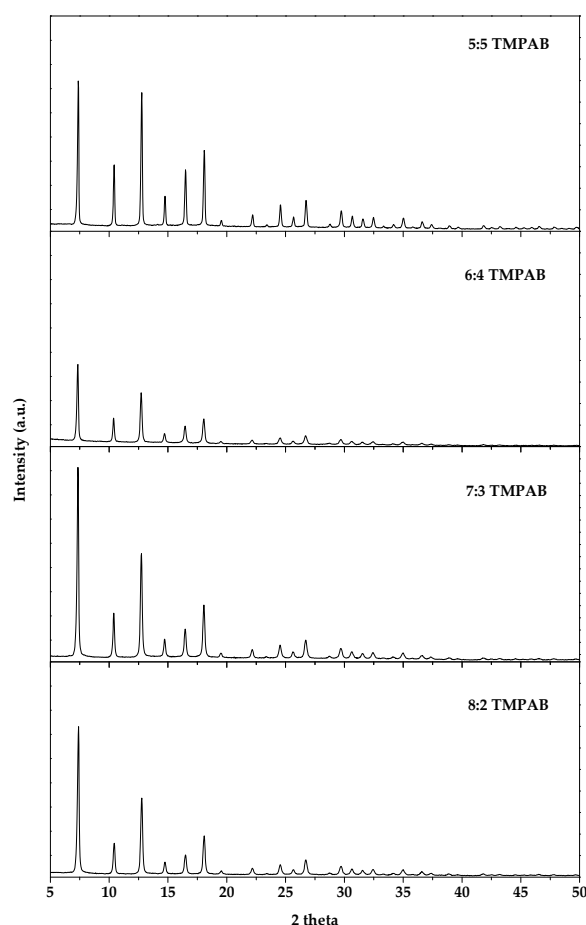


Figure 6. XRD patterns of synthesized ZIF-8 with TMPAB at a ratio between 2-MeIm and TMPAB as 5: 5, 6: 4, 7: 3 and 8: 2.

3.2. Modification of Synthesized ZIF-8 by Solvent-assisted Ligand Exchange

3.2.1. XRD and SEM

Synthesized ZIF-8 obtained from TMPAB with the ratio of 8:2 was selected to be used for modification by solvent-assisted ligand exchange method. The 2-methyl imidazole linker was replaced by two imidazole derivatives (2-NH₂bZIM and 2-PhIM). The molar ratio between synthesized ZIF-8 and imidazole derivatives was varied at 1:1, 1:3 and 1:5. Figure 9a,b illustrate XRD patterns of modified ZIF-8 by exchanging with 2-NH₂bZIM and 2-PhIM, respectively. A modified ZIF-8 with both imidazole derivatives exhibited the ZIF-8 characteristic peaks, which indicated that the ZIF-8 framework was preserved upon replacing 2-MeIm with two imidazole derivatives. Upon increasing the imidazole derivatives, the ZIF-8 structure remained unchanged while the peak intensities were different, which indicated different crystallinities of ZIF-8 crystals.

Figure 10 displays SEM images of exchanged ZIF-8 with 2-NH₂bZIM (Figure 10a) and 2-PhIM (Figure 10b) at various ratios between ZIF-8 and two imidazole derivatives. All samples exhibited larger particle sizes upon exchanging with two imidazole derivatives, i.e., the particle size of original ZIF-8 was around 400–600 nm, while those of all exchanged samples were in the range of 600–1500 nm. A few changes in the particle shapes were observed which was due to agglomeration.

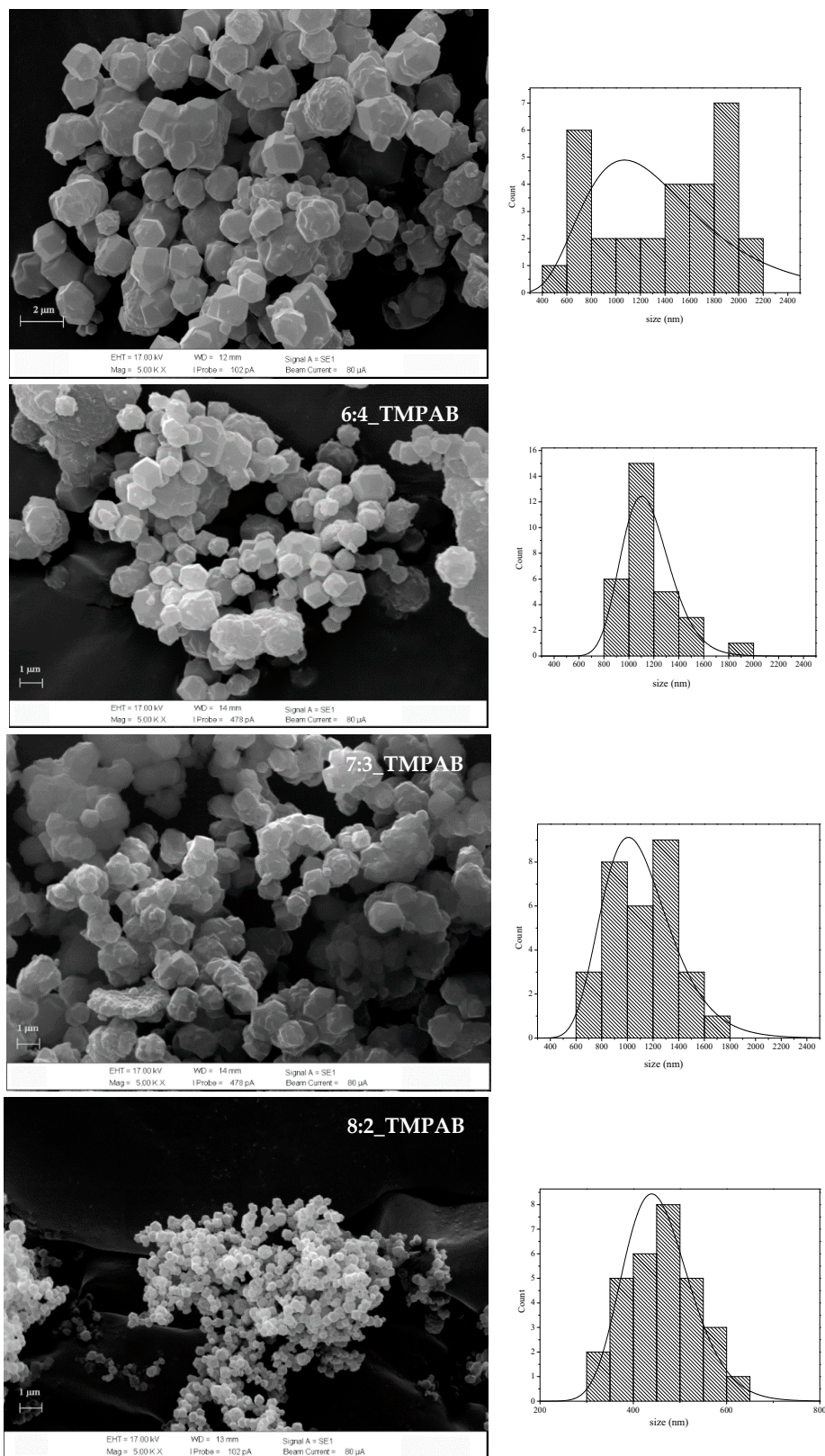


Figure 7. SEM images of synthesized ZIF-8 with various ratios between 2-MeIm and TMPAB.

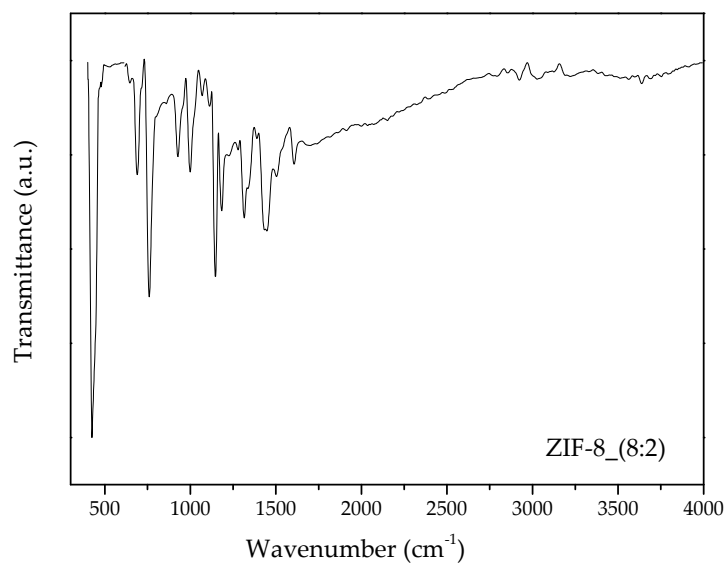


Figure 8. Fourier transform infrared (FTIR) of synthesized ZIF-8 obtained from optimal synthesis condition with the ratio between 2-MeIM and TMPAB as 8:2.

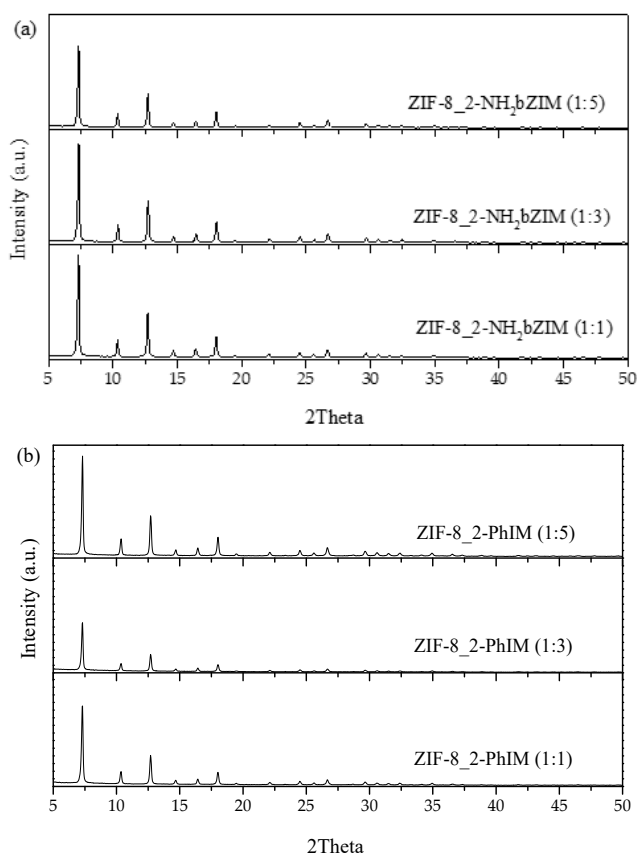
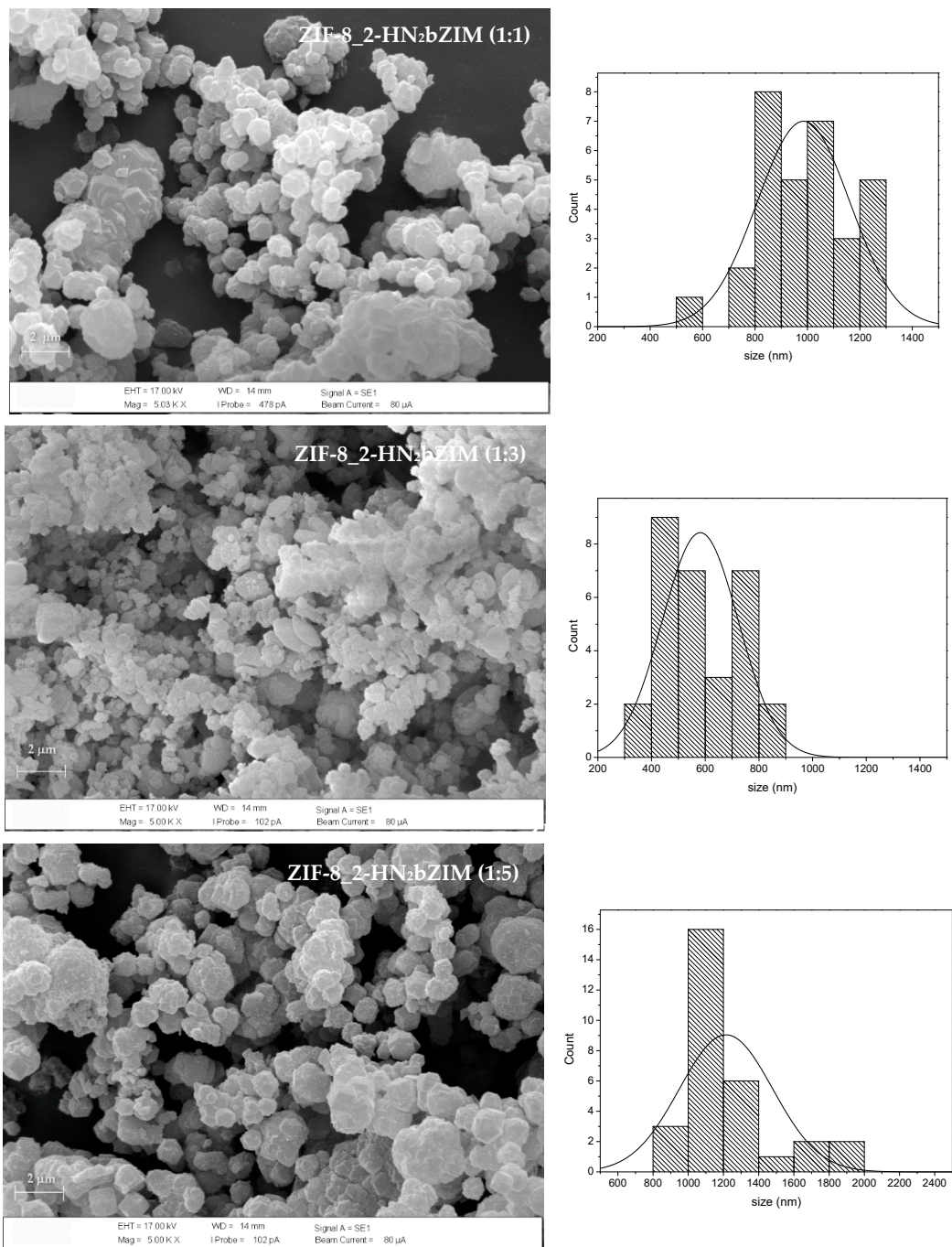


Figure 9. XRD patterns of modified ZIF-8 exchanged by (a) 2-aminobenzimidazole (2-NH₂bZIM) and (b) 2-phenylimidazole (2-PhIM) with various ratios between ZIF-8 and exchanged imidazole derivatives.



(a)

Figure 10. Cont.

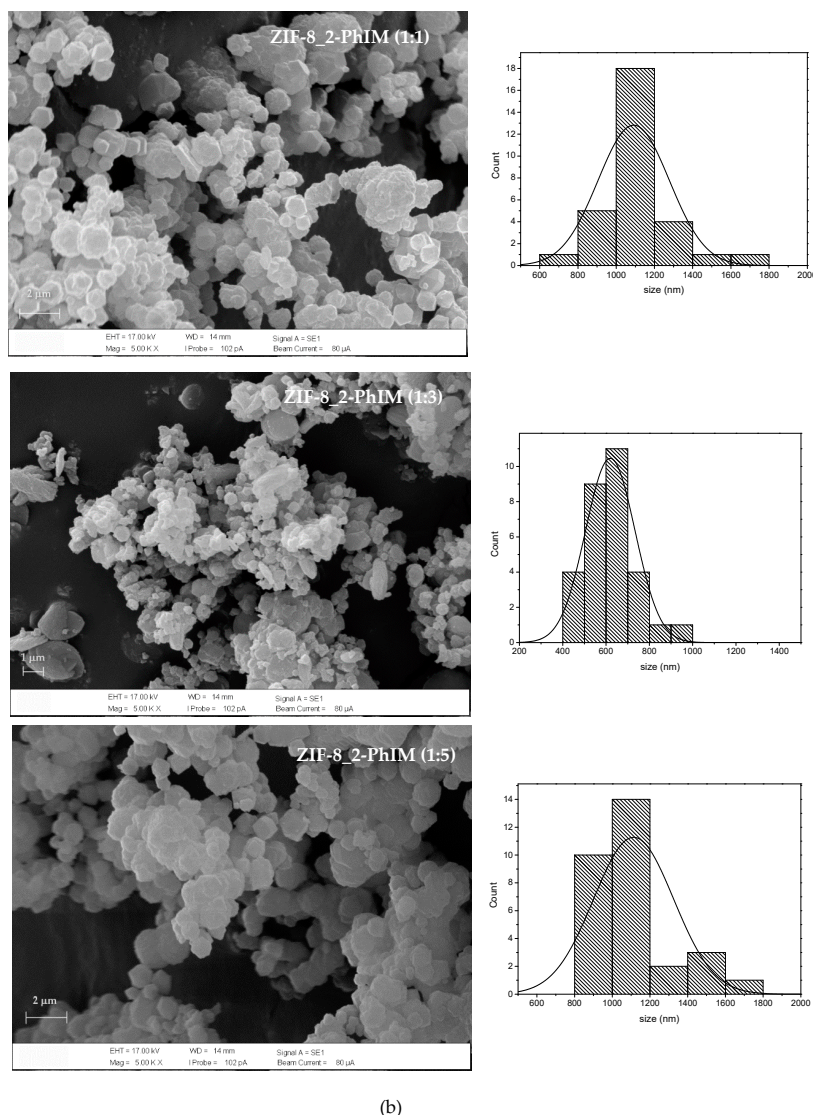


Figure 10. (a) Exchanged ZIF-8 samples for 2-NH₂bZIM linker at various ratio between ZIF-8 and 2-NH₂bZIM. (b) Exchanged ZIF-8 samples for 2-PhIM linker at various ratio between ZIF-8 and 2-PhIM.

3.2.2. ¹H NMR Analysis for the Replacement of Organic Linkers

In this section, ZIF-8 sample with the ratio of 1:3 was studied to confirm the replacement of 2-MeIM linker in ZIF-8 by 2-aminobenzimidazole and 2-phenylimidazole by the analysis of ¹H NMR spectral data (Figures 11–13). The signals at around 2.15 and 11.52 ppm which appeared in all samples were CH₃ and OH protons of digestive solvent, acetic acid-*d*₄. In Figure 11, spectral 11A demonstrated the ZIF-8 which clearly showed the key combination signals of N-CH₃ and sets of aromatic protons (3.40, and 7.58, 7.65 and 7.75 ppm) of TMPAB salt and CH₃ and CH=CH (2.55 and 7.50 ppm) of 2-MeIM, which corresponded to spectral 11B and 11C. It is worthy to note that the TMPAB salt signals in all samples were shifted compared to the pure TMPAB salt (3.90, 7.68, 7.74 and 8.16 ppm, spectral 11B). This is due to the environmental changes that caused the shielding of TMPAB proton signals. For the 2-aminobenzimidazole exchanged sample (Figure 12, spectral 12A), the characteristic proton signals of 2-MeIM were clearly observed (2.55 and 7.50 ppm). Additionally, it showed phenyl proton signals of 2-NH₂bZIM (7.31 and 7.49 ppm), which are comparable to spectral 12C. This indicated that 2-MeIM was replaced by 2-NH₂bZIM during the SALE process. The relative ratio of ZIF-8 and exchanged ZIF-8 by 2-NH₂bZIM was 1:0.11, based on the integration ratio of CH=CH protons of 2-MeIM (7.50 ppm, 2H) and the two ortho phenyl protons (7.31 ppm, 2H) of 2-NH₂bZIM. It is also revealed in

spectral 12A that the TMPAB salt signal intensity was decreased when compared to spectral 12B (7.65 and 7.75 ppm). The TMPAB salt may be removed during washing step of preparation process. For 2-phenylimidazole (Figure 13, spectral 13A), again the signals of 2-MeIM were observed (2.55 and 7.50 ppm). The key signals of ortho-substituted protons (2',6') and imidazole aromatic protons (4, 5) were observed at 8.10 and 7.72 ppm, which confirmed that 2-MeIM was replaced by 2-PhIM in SALE process. The approximately exchanged ratio was 1:0.04, based on the integration ratio of CH=CH protons of 2-MeIM (7.50 ppm, 2H) and the ortho-substituted protons (8.10 ppm, 2H) of 2-PhIM. In addition, the TMPAB salt signals were decreased when compared with spectral 13B (3.40 and 7.65 ppm).

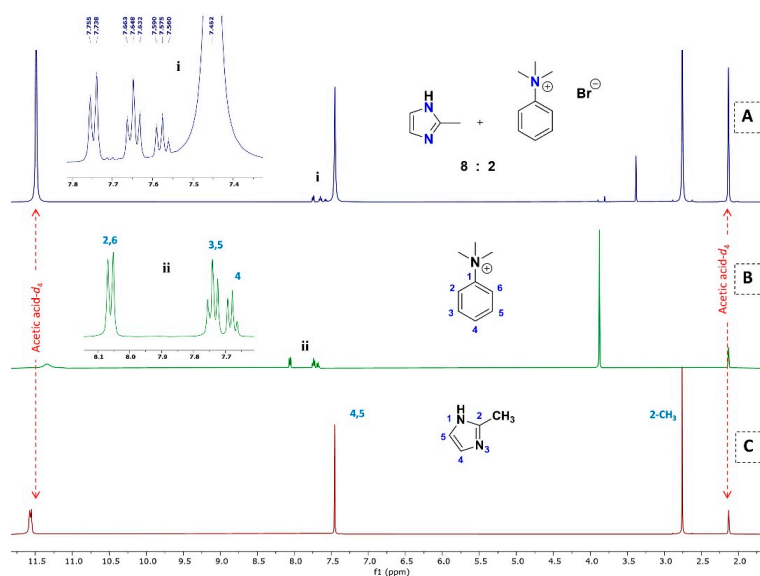


Figure 11. ^1H NMR spectra (in CD_3COOD) of (A) ZIF-8, (B) TMPAB salt and (C) 2-methylimidazole.

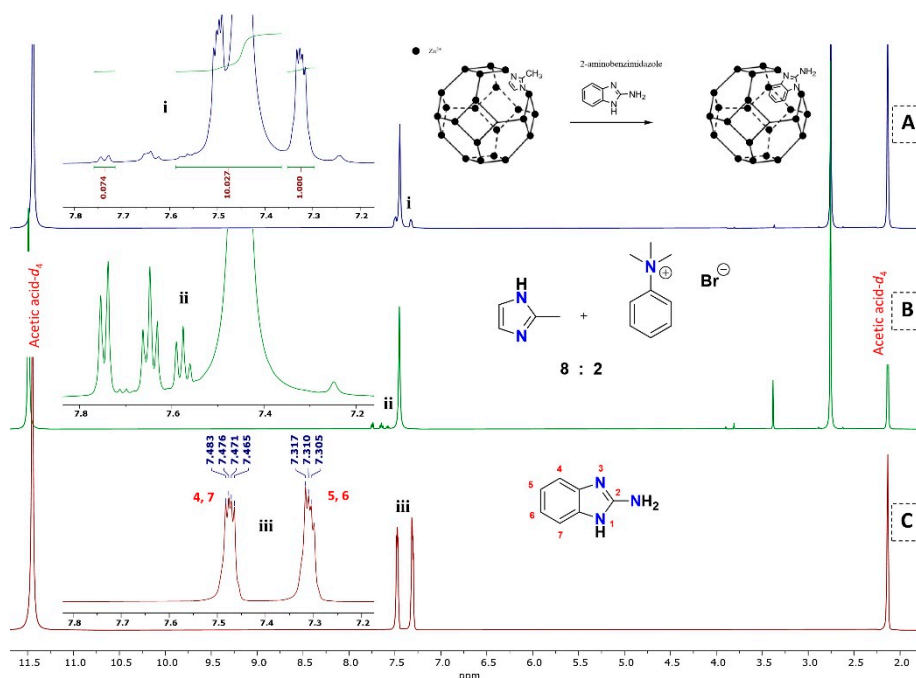


Figure 12. ^1H NMR spectra (in CD_3COOD) of (A) exchanged ZIF-8 sample by 2- NH_2bZIM (1:3), (B) ZIF-8 and (C) 2-aminobenzimidazole.

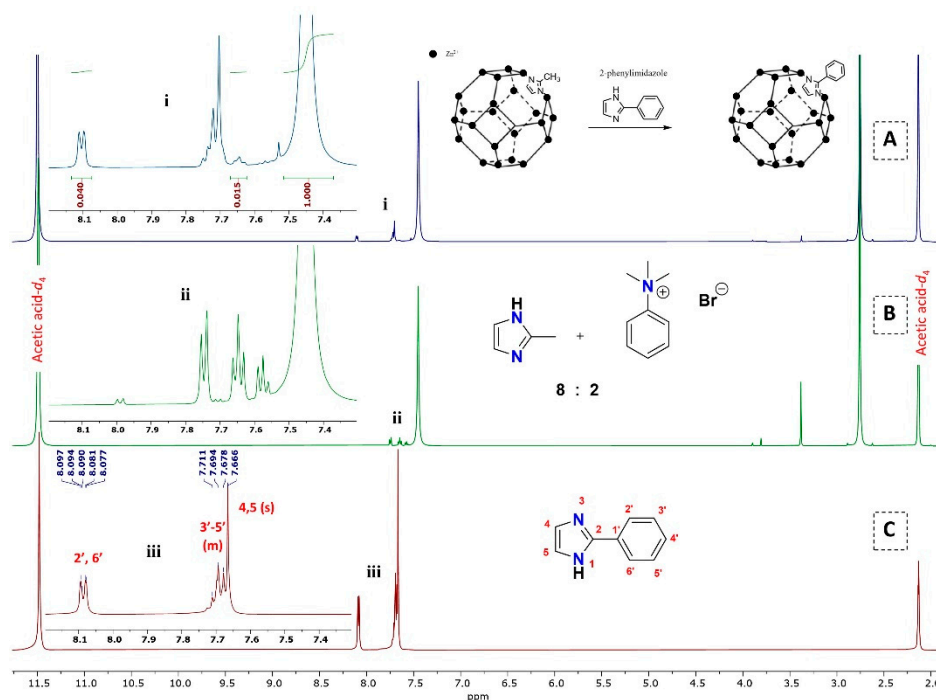


Figure 13. ^1H NMR spectra (in CD_3COOD) of (A) exchanged ZIF-8 sample by 2-PhIM (1:3), (B) ZIF-8 and (C) 2-phenylimidazole.

3.3. CO_2 Uptake

3.3.1. CO_2 Uptake of ZIF-8 Synthesized from Water based Synthesis Assisted by Hydrogen Bond Acceptors

The CO_2 uptake of all synthesized samples was measured by thermogravimetric analysis at 313 K and ambient pressure which were plotted as a function of time, as illustrated in Figure 14. The synthesized ZIF-8 with different ratios between 2-MeIM and TMPAB exhibited slightly different degree of CO_2 uptake abilities. The synthesized ZIF-8 sample with a ratio of 8:2 exhibited the highest CO_2 uptake when compared with other samples and the uptake amount was around 0.3 mmol/g at the adsorption time of 95 min. The CO_2 uptake of all samples was in the order of ZIF-8 (8:2) > ZIF-8 (7:3) > ZIF-8 (6:4) > ZIF-8 (5:5), which corresponded with the results of SEM, in that the particle size increased with a decrease in QAS content, i.e., the lower CO_2 uptake, the larger ZIF-8 particle sizes. The CO_2 uptake of ZIF-8 obtained by solvothermal method was also compared in Figure 14. It can be seen that the CO_2 uptake of ZIF-8 from the solvothermal method exhibited much higher CO_2 uptake than ZIF-8 synthesized from TMPAB (the water based synthesis method). The CO_2 adsorption behavior and CO_2 adsorption mechanism will be discussed in the next part.

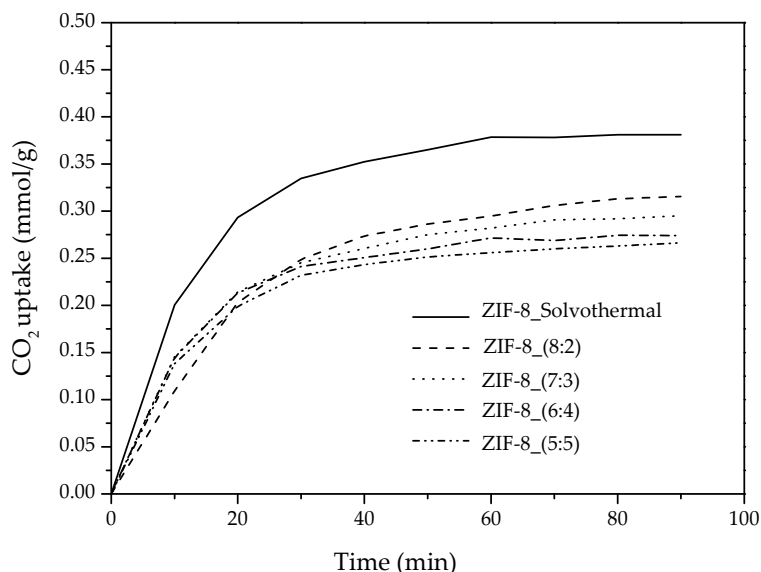


Figure 14. CO₂ uptake of ZIF-8 samples at different ratios between 2-MeIM and TMPAB compared with ZIF-8 synthesized by solvothermal method at 313 K.

3.3.2. CO₂ Uptake of Exchanged ZIF-8 by Imidazole Derivatives

Figure 15a,b illustrate CO₂ uptake of modified ZIF-8 by exchanging with 2-aminobenzimidazole and 2-phenylimidazole, respectively. The 2-NH₂bZIM and 2-PhIM exchanged samples with different ratios between ZIF-8 and these two imidazole derivatives were also compared with the original synthesized ZIF-8. Upon exchanging the 2-MeIM of ZIF-8 by 2-NH₂bZIM and 2-PhIM, the CO₂ uptake was improved. The results also revealed that the increasing ratio of both imidazole derivatives have a slightly impact on the CO₂ uptake of samples. Therefore, the ZIF-8 sample with the ratio of 1:3 was selected for further discussion of the CO₂ adsorption behavior in the exchanged sample.

3.3.3. CO₂ Adsorption Mechanism

Figure 16 shows the CO₂ uptake of ZIF-8 and two ZIF-8 exchanged samples obtained from the water based synthesis method, and ZIF-8 obtained from the solvothermal method. It is clearly seen that upon exchanging the 2-MeIM linker with imidazole derivatives, the CO₂ uptake was enhanced. In order to explain the CO₂ uptake ability of synthesized ZIF-8 by hydrogen bond acceptor assisted and linker exchanged samples, data analysis of the surface properties for those samples were performed. Figure 17 shows N₂ adsorption desorption of original ZIF-8 (with the ratio of 8:2) and exchanged ZIF-8 by two imidazole derivatives. All isotherms exhibited a type I adsorption isotherm. The adsorption of N₂ was steeply increased at low relative pressure which suggested the existence of micropore. Table 1 shows summary data of surface area, average pore size and pore volume of the synthesized samples. In the case of exchanged ZIF-8 samples with 2-NH₂bZIM and 2-PhIM ligands, the surface areas were enhanced when compared with the original ZIF-8. However, 2-NH₂bZIM and 2-PhIM were bulkier than the original ligand (2-MeIM), thus the exchanging of those led to less accessible porosity due to the blocking of the exchanged linkers. In addition, the increase in surface area upon exchanging with the new ligands might be due to the removal of trapped TMPAB from the pores during the exchanged process. Therefore, to prove this assumption, the blank experiment was conducted by exchanging ZIF-8 by the same procedure without adding the imidazole derivatives. It was found that the surface area of blank sample was 1470.1 m²/g. This indicated that increase in surface area upon exchanging with imidazole derivatives was due to the removal of some TMPAB from the pores.

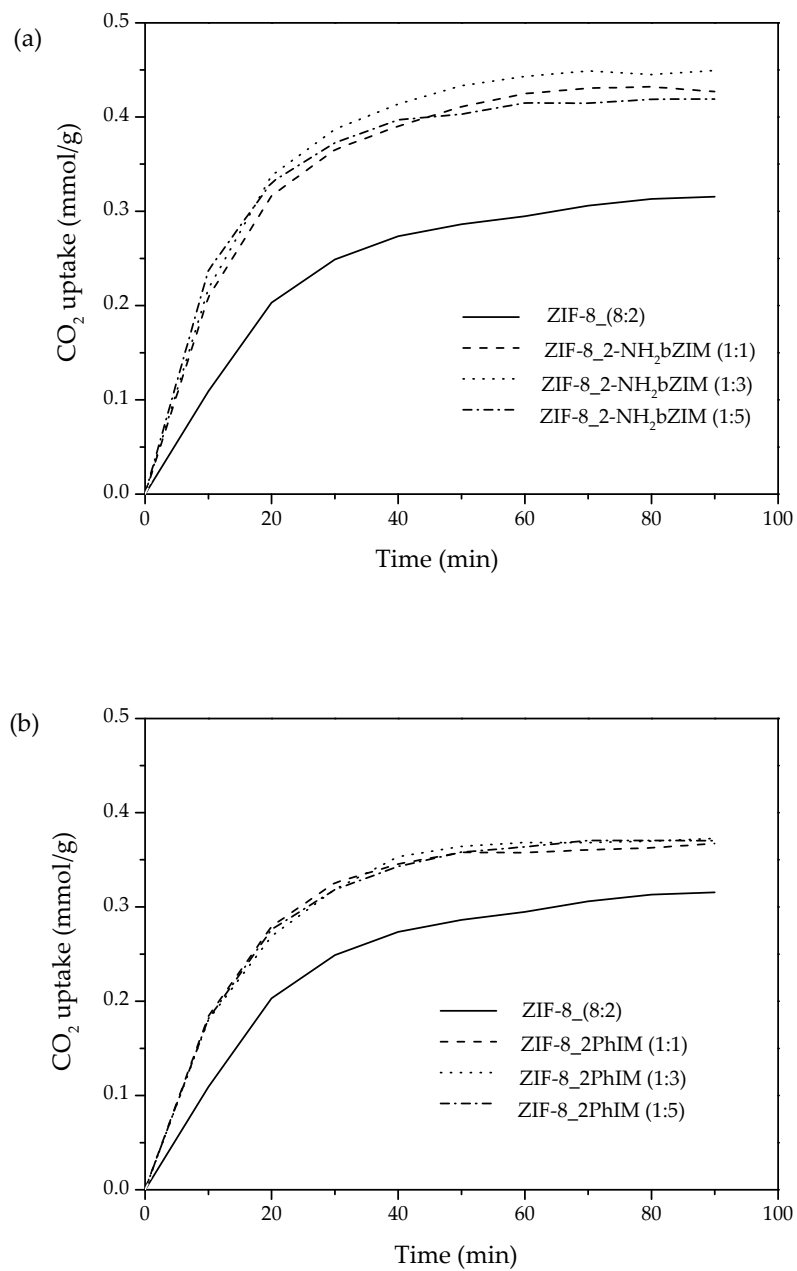


Figure 15. CO₂ uptake of synthesized ZIF-8 modified by (a) 2-aminobenzimidazole and (b) 2-phenylimidazole with different ratios between ZIF-8 and exchanged imidazole at 313 K.

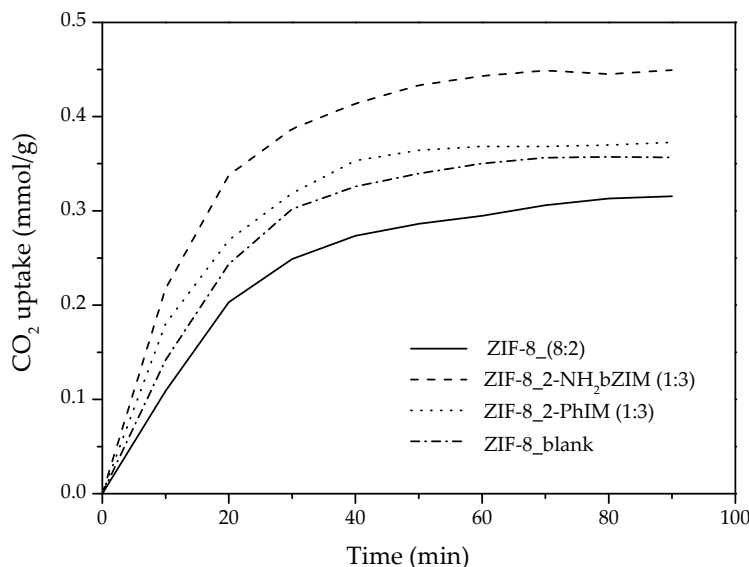


Figure 16. Comparison of CO₂ uptake of synthesized ZIF-8 by water based synthesis with hydrogen bond acceptor assisted and exchanged ZIF-8 at 313 K.

Between ZIF-8 (8:2) and ZIF-8-blank samples, based on the assumption that TMPAB was completely removed from the samples, the enhancing of CO₂ uptake may be due to the increasing of internal surface area. For the 2-NH₂bZIM exchanged sample, it exhibited a higher CO₂ uptake than that of the original ZIF-8 and ZIF-8-blank samples (Figure 16). As describe above that higher surface area of exchanged ZIF-8 samples were due to the removal of some TMPAB from the sample during the exchanged process, and consequently the amount of CO₂ uptake of exchanged samples should be lower than ZIF-8-blank sample. Therefore, higher CO₂ uptake of exchanged samples indicated that increase in surface area was not the main factor to dominate the CO₂ uptake. This enhancing of CO₂ uptake was probably due to some additional interaction between the exchanged linker and some TMPAB with CO₂. The CO₂ uptake of the 2-NH₂bZIM exchanged sample was higher than that of 2-PhIM-exchanged and ZIF-8-blank samples, due to a higher amount of exchanged 2-NH₂bZIM (around 11% from ¹H-NMR analysis). This enhancing of CO₂ uptake was due to additional interaction between CO₂ and the amine group of 2-NH₂bZIM. The increased in CO₂ uptake can be attributed to two factors. First, the basic amino groups have a high affinity toward an acidic CO₂ molecule. These results are in agreement with L. Xiang et al. [42], who reported the synthesized amino-functionalization by the *in-situ* substitution of 2-NH₂bZIM into the ZIF-7. The results show that the CO₂ uptake of the amino-functionalization sample was higher than that of pristine ZIF-8. They proposed that the higher CO₂ uptake was probably due to the CO₂ affinity of the polar amino group on amino-modified ZIF-8 framework. The second factor was the quadrupole- π electron interaction between the CO₂ molecule and the imidazole and/or phenyl ring in 2-NH₂bZIM, which was strengthened by the electron-donating group (amino functional group) [43]. Accordingly, the TMPAB in all samples may also promote the CO₂ uptake by the interaction between the delocalized π -aromatic system of the phenyl group and CO₂. In contrast, the lower exchanged amount of 2-PhIM (around 4% from ¹H-NMR analysis) led to nearly the same amount of CO₂ uptake to ZIF-8-blank sample, which may be due to higher surface area of this exchanged sample being dominant in the CO₂ uptake behavior.

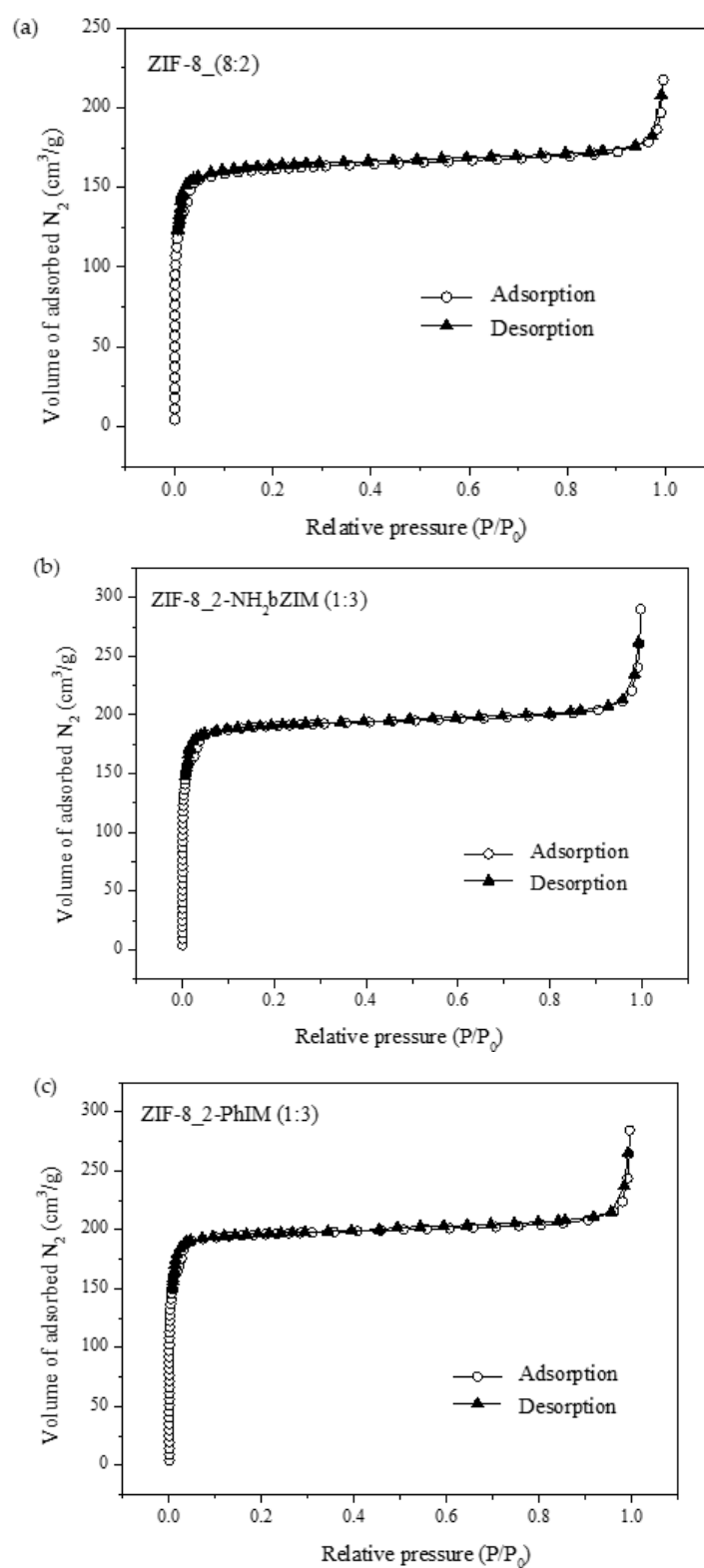


Figure 17. (a) N_2 adsorption-desorption isotherms of ZIF-8 obtained from water based synthesis with hydrogen bond acceptor assisted, (b) exchanged ZIF-8 by 2-NH₂bZIM and (c) 2-PhIM, respectively.

Table 1. Surface area, pore diameter and pore volume of synthesized samples.

Sample	Surface Area (m ² /g)	Average Pore Diameter (nm)	Pore Volume (cm ³ /g)
ZIF-8_Solvothermal	1539	2.280	0.6469
ZIF-8_(8:2)	634.0	1.920	0.3043
ZIF-8_2-NH ₂ bZIM(1:3)	745.2	1.985	0.3698
ZIF-8_2-PhIM (1:3)	775.8	1.928	0.3739

4. Conclusions

In this work, a zeolitic imidazolate framework-8 (ZIF-8) was synthesized by the water based synthesis method with hydrogen bond acceptor assisted and modified ZIF-8 by solvent-assisted ligand exchange method to enhance the CO₂ adsorption performance. Several synthesis conditions were investigated. The effects of mixed ordering steps of precursors showed that the mixing of 2-MeIM and quaternary ammonium salts (QAS) before adding Zn(NO₃)₂·6H₂O solution provided a ZIF-8 with high crystallinity. The quaternary ammonium salts were varied by using three different compounds: tetraethylammonium bromide (TEAB), tetrabutylammonium bromide (TBAB) and trimethyl phenyl ammonium bromide (TMPAB). The results show that ZIF-8 synthesized by forming in TMPAB exhibited good size distribution and the smallest particle sizes compared with two other QAS. This can be explained by the higher hydrogen bonding strength of 2-MeIM and TMPAB, which led to an increase in the 2-MeIM deprotonation rate, which then sped up the coordination of linker with Zn²⁺ ion. This effect can lead to a high nucleation rate and crystal growth of ZIF-8, which also led to uniformly distributed ZIF-8 particles. Moreover, the effects of various ratios between 2-MeIM and TMPAB were also studied. The ratio of 8:2 provided a good distribution of ZIF-8 particles and the smallest particle size was also obtained. Therefore, the optimal synthesis conditions were using TMPAB as a QAS with a ratio between 2-MeIM and TMPAB of 8:2 and when TMPAB was first mixed with 2-MeIM before the Zn(NO₃)₂·6H₂O solution was added. The synthesized ZIF-8 was then modified by solvent-assisted ligand exchange methods to enhance the CO₂ uptake. The 2-MeIM linker in ZIF-8 was exchanged by two imidazole derivatives: 2-aminobenzimidazole (2-NH₂bZIM) and 2-phenylimidazole (2-PhIM). The CO₂ uptake was carried out by thermogravimetric analysis (TGA) at atmospheric pressure. The results show that exchanged ZIF-8 samples with 2-NH₂bZIM exhibited higher CO₂ uptake than that of pristine ZIF-8 due to two factors; i.e., (i) an additional interaction between CO₂ and exchanged imidazole derivatives and (ii) increasing surface area, pore size and pore volume upon exchanging with the imidazole derivative.

Author Contributions: The present research project has been initiated by K.K. and K.C.C.; sample preparation and characterization by K.K.; writing—original draft preparation by K.C.C.; ¹H-NMR interpretation by S.M. and P.J. All authors have read and agreed to the published version of the manuscript.

Funding: This research received no external funding.

Acknowledgments: The authors gratefully acknowledge the facility support from Faculty of Science, Khon Kaen University, Thailand. This work was financially supported by the Science Achievement Scholarship of Thailand (SAST).

Conflicts of Interest: The authors declare no conflict of interest.

References

- Xu, G.; Li, L.; Yang, Y.; Tian, L.; Liu, T.; Zhang, K. A novel CO₂ cryogenic liquefaction and separation system. *Energy* **2012**, *42*, 522–529. [[CrossRef](#)]
- Knapiak, E.; Kosowski, P.; Stopa, J. Cryogenic liquefaction and separation of CO₂ using nitrogen removal unit cold energy. *Chem. Eng. Res. Des.* **2018**, *131*, 66–79. [[CrossRef](#)]

3. Maqsood, K.; Mullick, A.; Ali, A.; Kargupta, K.; Ganguly, S. Cryogenic carbon dioxide separation from natural gas: A review based on conventional and novel emerging technologies. *Rev. Chem. Eng.* **2014**, *30*, 453–477. [[CrossRef](#)]
4. Brunetti, A.; Scura, F.; Barbieri, G.; Drioli, E. Membrane technologies for CO₂ separation. *J. Membr. Sci.* **2010**, *359*, 115–125. [[CrossRef](#)]
5. Rezakazemi, M.; Amooghin, A.E.; MehdiMontazer-Rahmati, M.; FauziIsmail, A.; Matsuura, T. State-of-the-art membrane based CO₂ separation using mixed matrix membranes (MMMs): An overview on current status and future directions. *Prog. Polym. Sci.* **2014**, *39*, 817–861. [[CrossRef](#)]
6. Xu, J.; Wu, H.; Wang, Z.; Qiao, Z.; Zhao, S.; Wang, J. Recent advances on the membrane processes for CO₂ separation. *Chin. J. Chem. Eng.* **2018**, *26*, 2280–2291. [[CrossRef](#)]
7. Rochelle, G.T. Amine scrubbing for CO₂ capture. *Science* **2009**, *325*, 1652–1654. [[CrossRef](#)]
8. Chen, P.C.; Lin, S.-Z. Optimization in the Absorption and Desorption of CO₂ Using Sodium Glycinate Solution. *Appl. Sci.* **2018**, *8*, 2041. [[CrossRef](#)]
9. Haider, M.B.; Hussain, Z.; Kumar, R. CO₂ absorption and kinetic study in ionic liquid amine blends. *J. Mol. Liq.* **2016**, *224*, 1025–1031. [[CrossRef](#)]
10. Mello, M.R.; Phanon, D.; Silveira, G.Q.; Llewellyn, P.L.; Ronconi, C.M. Amine-modified MCM-41 mesoporous silica for carbon dioxide capture. *Microporous Mesoporous Mater.* **2011**, *143*, 174–179. [[CrossRef](#)]
11. Younas, M.; Sohail, M.; Leong, L.K.; Bashir, M.J.K.; Sumathi, S. Feasibility of CO₂ adsorption by solid adsorbents: A review on low-temperature systems. *Int. J. Environ. Sci. Technol.* **2016**, *13*, 1839–1860. [[CrossRef](#)]
12. Wang, J.; Huang, L.; Yang, R.; Zhang, Z.; Wu, J.; Gao, Y.; Wang, Q.; O'Hare, D.; Zhong, Z. Recent advances in solid sorbents for CO₂ capture and new development trends. *Energy Environ. Sci.* **2014**, *7*, 3478–3518. [[CrossRef](#)]
13. Chen, C.; Ahn, W.S. CO₂ adsorption on LTA zeolites: Effect of mesoporosity. *Appl. Surf. Sci.* **2014**, *311*, 107–109. [[CrossRef](#)]
14. Gunawan, T.; Wijiyanti, R.; Widiastuti, N. Adsorption–desorption of CO₂ on zeolite-Y-templated carbon at various temperatures. *RSC Adv.* **2018**, *8*, 41594–41602. [[CrossRef](#)]
15. Megías-Sayago, C.; Bingre, R.; Huang, L.; Lutzweiler, G.; Wang, Q.; Louis, B. CO₂ Adsorption Capacities in Zeolites and Layered Double Hydroxide Materials. *Front. Chem.* **2019**, *7*, 551. [[CrossRef](#)]
16. Hu, J.; Liu, Y.; Liu, J.; Gu, C.; Wu, D. High CO₂ adsorption capacities in UiO type MOFs comprising heterocyclic ligand. *Microporous Mesoporous Mater.* **2018**, *256*, 25–31. [[CrossRef](#)]
17. Kukulka, W.; Cendrowski, K.; Michalkiewicz, B.; Mijowska, E. MOF-5 derived carbon as material for CO₂ absorption. *RSC Adv.* **2019**, *9*, 18527–18537. [[CrossRef](#)]
18. Kochetygov, I.; Bulut, S.; Asgari, M.; Queen, W.L. Selective CO₂ adsorption by a new metal–organic framework: Synergy between open metal sites and a charged imidazolium backbone. *Dalton Trans.* **2018**, *47*, 10527–10535. [[CrossRef](#)]
19. Khan, I.U.; Othman, M.H.D.; Jilani, A.; Ismail, A.F.; Hashim, H.; Jaafar, J.; Rehman, G.U. Economical, environmental friendly synthesis, characterization for the production of zeolitic imidazolate framework-8 (ZIF-8) nanoparticles with enhanced CO₂ adsorption. *Arab. J. Chem.* **2018**, *11*, 1072–1083. [[CrossRef](#)]
20. Song, F.; Cao, Y.; Zhao, Y.; Jiang, R.; Xu, Q.; Yan, J.; Zhong, Q. Ion-Exchanged ZIF-67 Synthesized by One-Step Method for Enhancement of CO₂ Adsorption. *J. Nanomater.* **2020**, 1508574. [[CrossRef](#)]
21. Arami-Niya, A.; Birkett, G.; Zhu, Z.; Rufford, T.E. Gate opening effect of zeolitic imidazolate framework ZIF-7 for adsorption of CH₄ and CO₂ from N₂. *J. Mater. Chem. A* **2017**, *5*, 21389–21399. [[CrossRef](#)]
22. Lee, Y.R.; Jang, M.S.; Cho, H.Y.; Kwon, H.J.; Kim, S.; Ahn, W.S. ZIF-8: A comparison of synthesis methods. *Chem. Eng. J.* **2015**, *271*, 276–280. [[CrossRef](#)]
23. Cravillon, J.; Schröder, C.A.; Bux, H.; Rothkirch, A.; Caro, J.; Wiebcke, M. Formate modulated solvothermal synthesis of ZIF-8 investigated using time-resolved in situ X-ray diffraction and scanning electron microscopy. *CrystEngComm* **2012**, *14*, 492–498. [[CrossRef](#)]
24. Sze, L.; Yin, L.; Yeong, F.; Keong, K.; Azmi, L.; Shariff, M. Effect of Synthesis Parameters on the Formation of ZIF-8 Under Microwave-assisted Solvothermal. *Procedia Eng.* **2016**, *148*, 35–42.
25. Sun, W.; Zhai, X.; Zhao, L. Synthesis of ZIF-8 and ZIF-67 nanocrystals with well-controllable size distribution through reverse microemulsions. *Chem. Eng. J.* **2016**, *289*, 59–64. [[CrossRef](#)]

26. Butova, V.V.; Budny, A.P.; Bulanova, E.A.; Lamberti, C.; Soldatov, A.V. Water based synthesis of high surface area ZIF-8 with minimal use of TEA. *Solid State Sci.* **2017**, *69*, 13–21. [[CrossRef](#)]
27. Oozeerally, R.; Ramkhelawan, S.D.K.; Burnett, D.L.; Tempelman, C.H.L.; Degirmenci, V. ZIF-8 Metal Organic Framework for the Conversion of Glucose to Fructose and 5-Hydroxymethyl Furfural. *Catalysts* **2019**, *9*, 812. [[CrossRef](#)]
28. Kida, K.; Okita, M.; Fujita, K.; Tanaka, S.; Miyake, Y. Formation of high crystalline ZIF-8 in an aqueous solution. *CrystEngComm* **2013**, *15*, 1794–1801. [[CrossRef](#)]
29. Gross, A.F.; Sherman, E.; Vajo, J.J. Aqueous room temperature synthesis of cobalt and zinc sodalite zeolitic imidazolate frameworks. *Dalton Trans.* **2012**, *41*, 5458–5460. [[CrossRef](#)]
30. Yao, J.; He, M.; Wang, K.; Chen, R.; Zhong, Z.; Wang, H. High-yield synthesis of zeolitic imidazolate frameworks from stoichiometric metal and ligand precursor aqueous solutions at room temperature. *CrystEngComm* **2013**, *15*, 3601–3606. [[CrossRef](#)]
31. Hu, L.; Chen, L.; Fang, Y.; Wang, A.; Chen, C.; Yan, Z. Facile synthesis of zeolitic imidazolate framework-8 (ZIF-8) by forming imidazole-based deep eutectic solvent. *Microporous Mesoporous Mater.* **2018**, *268*, 207–215. [[CrossRef](#)]
32. Karagiari, O.; Lalonde, M.B.; Bury, W.; Sarjeant, A.A.; Farha, O.K.; Hupp, J.T. Opening ZIF-8: A catalytically active zeolitic imidazolate framework of sodalite topology with unsubstituted linkers. *J. Am. Chem. Soc.* **2012**, *134*, 18790–18796. [[CrossRef](#)] [[PubMed](#)]
33. Stephenson, C.J.; Hupp, J.T.; Farha, O.K. Postassembly Transformation of a Catalytically Active Composite Material, Pt@ ZIF-8, via Solvent-Assisted Linker Exchange. *Inorg. Chem.* **2016**, *55*, 1361–1363. [[CrossRef](#)] [[PubMed](#)]
34. Kim, S.; Dawson, K.W.; Gelfand, B.S.; Taylor, J.M.; Shimizu, G.K. Enhancing proton conduction in a metal–organic framework by isomorphous ligand replacement. *J. Am. Chem. Soc.* **2013**, *135*, 963–966. [[CrossRef](#)] [[PubMed](#)]
35. Pullen, S.; Fei, H.; Orthaber, A.; Cohen, S.M.; Ott, S. Enhanced photochemical hydrogen production by a molecular diiron catalyst incorporated into a metal–organic framework. *J. Am. Chem. Soc.* **2013**, *135*, 16997–17003. [[CrossRef](#)]
36. Bury, W.; Fairen-Jimenez, D.; Lalonde, M.B.; Snurr, R.Q.; Farha, O.K.; Hupp, J.T. Control over catenation in pillared paddlewheel metal–organic framework materials via solvent-assisted linker exchange. *Chem. Mater.* **2013**, *25*, 739–744. [[CrossRef](#)]
37. Tsai, C.W.; Niemantsverdriet, J.W.; Langner, E.H. Enhanced CO₂ adsorption in nano-ZIF-8 modified by solvent assisted ligand exchange. *Microporous Mesoporous Mater.* **2018**, *262*, 98–105. [[CrossRef](#)]
38. Laurence, C.; Berthelot, M. Observations on the strength of hydrogen bonding. *Perspect. Drug Discov. Des.* **2000**, *18*, 39–60. [[CrossRef](#)]
39. Levitt, M.; Perutz, M.F. Aromatic rings act as hydrogen bond acceptors. *J. Mol. Biol.* **1988**, *201*, 751–754. [[CrossRef](#)]
40. Zhang, Y.; Jia, Y.; Hou, L. Synthesis of zeolitic imidazolate framework-8 on polyester fiber for PM2.5 removal. *RSC Adv.* **2018**, *8*, 31471–31477. [[CrossRef](#)]
41. Tanaka, S.; Tanaka, Y. Simple Step toward Enhancing Hydrothermal Stability of ZIF-8. *ACS Omega* **2019**, *4*, 19905–19912. [[CrossRef](#)] [[PubMed](#)]
42. Xiang, L.; Sheng, L.; Wang, C.; Zhang, L.; Pan, Y.; Li, Y. Amino-Functionalized ZIF-7 Nanocrystals: Improved Intrinsic Separation Ability and Interfacial Compatibility in Mixed-Matrix Membranes for CO₂/CH₄ Separation. *Adv. Mater.* **2017**, *29*, 1606999. [[CrossRef](#)] [[PubMed](#)]
43. Liu, D.; Wu, Y.; Xia, Q.; Li, Z.; Xi, H. Experimental and molecular simulation studies of CO₂ adsorption on zeolitic imidazolate frameworks: ZIF-8 and amine-modified ZIF-8. *Adsorption* **2013**, *19*, 25–37. [[CrossRef](#)]

